

DOI: 10.1002/cssc.201000002

Advanced Materials from Natural Materials: Synthesis of Aligned Carbon Nanotubes on Wollastonites

Meng-Qiang Zhao, Qiang Zhang, Jia-Qi Huang, Jing-Qi Nie, and Fei Wei^{*,[a]}

The growth of carbon nanotubes (CNTs) on natural materials is a low-cost, environmentally benign, and materials-saving method for the large-scale production of CNTs. Directly building 3D CNT architectures on natural materials is a key issue for obtaining advanced materials with high added value. We report the fabrication of aligned CNT arrays on fibrous natural wollastonite. Strongly dispersed iron particles with small sizes were produced on a planar surface of soaked fibrous wollastonite by a reduction process. These particles then catalyzed

the decomposition of ethylene, leading to the synchronous growth of CNTs to form leaf- and brush-like wollastonite/CNT hybrids. The as-obtained hybrids could be further transformed into porous SiO₂/CNT hybrids by reaction with hydrochloric acid. Further treatment with hydrofluoric acid resulted in aligned CNT arrays, with purities as high as 98.7%. The presented work is very promising for the fabrication of advanced materials with unique structures and properties that can be used as fillers, catalyst supports, or energy-absorbing materials.

Introduction

The production of advanced materials from natural materials can contribute to diminishing our current dependence on non-renewable feedstocks.^[1,2] Carbon nanotubes (CNTs), which can be conceptually viewed as graphene sheets that are rolled into a nanometer-scale tube form, are a class of attractive nanomaterials. Depending on their diameter, helicity, and alignment along the *c*-axis, CNTs exhibit extraordinary behaviors that allow them to be used for many potential applications, including as energy conversion components of fuel cells or lithium-ion secondary batteries;^[3,4] engineering materials to enhance the electrical and electrostatic properties or tenacity of polymers, textiles, metals, and coatings;^[5] catalysts for oxidative dehydrogenation;^[6,7] carriers of Fischer–Tropsch, noble-metal hydrogenation, or other catalysts;^[8] and field emission displays.^[9] For most of the above-mentioned and many other applications, it is highly desirable to prepare aligned CNTs. Indeed, compared with entangled CNTs, vertically aligned CNTs (VACNTs) have a good orientation, large aspect ratio, and high purity. It has been widely recognized that among the various forms of CNTs, aligned CNTs can be considered advanced materials of paramount importance for most of the above-mentioned applications.^[4,9] An efficient method for the low-cost mass production of aligned CNTs is required for their large-scale application.

Recently, several natural materials have been used for the synthesis of nanomaterials with the aim of developing low-cost, environmentally benign, and materials-saving processes.^[11] Volcanic lava rock,^[6,10] soil,^[11] garnet sand,^[11] bentonite,^[12] sepiolite,^[13] forsterite,^[14] disporide,^[14] and biomass-based activated carbon^[15] can be used as catalysts for the growth of CNTs. Montmorillonite^[16] and fly ash^[17] can serve as catalyst supports for CNT synthesis as well. Natural materials originating from biomass, such as coal,^[18] natural gas,^[11] liquefied petroleum gas,^[19] or biomass itself,^[20] can be used as carbon sources for

CNT synthesis. The as-obtained products grown from natural materials performed very well as catalysts in oxidative dehydrogenation (carbon nanofiber/lava^[6] and CNT/bentonite^[12]), for energy absorption (alternating aligned CNTs and vermiculite layers),^[21] and as fillers for strong polyamide-6 composites (CNT/clay hybrids).^[22] Making use of natural materials for the synthesis of nanomaterials can be considered as an example of sustainable chemistry and materials science. These eco-friendly methods are very interesting because they allow the large-scale production of CNTs at low costs.

However, there still are some disadvantages when natural materials are used for the synthesis of nanomaterials. For example, most of the CNT products grown on natural materials have a wide distribution of diameters. CNTs in the as-grown products are usually strongly entangled.^[6,10–17] Recently, Zhang et al. reported the intercalated growth of aligned CNTs on natural clays, such as vermiculite and mica, and the as-obtained CNT/clay hybrids could serve as an advanced material for shock-absorbing applications.^[21] The synthesis of advanced CNT materials on natural materials, with good alignment, uniform diameters, and homogeneous structures, remains a challenge.

Herein, wollastonite, a mineral that exhibits a fibrous structure in the form of needle-shaped crystals, is used as natural substrate for the facile synthesis of aligned CNTs. Wollastonite is a type of calcium inosilicate (CaSiO₃) that is widely available from commercial mining in PR China, USA, India, Finland,

[a] Dr. M.-Q. Zhao, Dr. Q. Zhang, J.-Q. Huang, J.-Q. Nie, Prof. F. Wei
Beijing Key Laboratory of
Green Chemical Reaction Engineering and Technology
Department of Chemical Engineering, Tsinghua University
100084 Beijing (PR China)
Fax: (+86) 10 6277-2051
E-mail: wf-dce@tsinghua.edu.cn

former Yugoslavia, Mexico, Greece, and other countries. Wollastonite exhibits many useful properties, such as a high brightness and whiteness, low absorption of moisture and oil, and a low content of volatiles. These characteristics form the basis for the widespread application of wollastonite in ceramic composites, paint, paper, plastics, and vinyl tile manufacture.^[23] We found that aligned CNTs can be easily synthesized on wollastonite fiber via chemical vapor deposition (CVD). The as-grown CNTs feature good alignment and narrow diameter and length distributions. Moreover, the as-grown CNT arrays can be easily purified to ca. 98.7%, providing a scaleable route towards high-value advanced materials with extraordinary performance.

Results and Discussion

The wollastonite catalyst for the growth of aligned CNTs

Wollastonite mined from PR China was directly used as catalyst support. Table 1 shows the composition of the pristine wollastonite as determined by X-ray fluorescence (XRF) analysis. The

Wollastonite component	Content [wt%]
SiO ₂	51.14
CaO	46.77
MgO	1.67
Fe ₂ O ₃	0.19
Al ₂ O ₃	0.08
SrO	0.05
Cr ₂ O ₃	0.05
Other	0.05

wollastonite contained 51.14 wt% SiO₂, 46.77 wt% CaO, and 1.67 wt% MgO. The natural Fe loading was 0.13 wt% (0.19 wt% Fe₂O₃), which is too low for the growth of aligned CNTs. Furthermore, the wollastonite contained small amounts of other oxides such as Al₂O₃, SrO, and Cr₂O₃.

Wollastonite usually crystallizes triclinically in space group *P* $\bar{1}$. Its mineralogical name is wollastonite-1T and is distinguished from the more rare monoclinic wollastonite-2M (space group *P*2₁). The structure of wollastonite-1T contains infinite alternant chains of [SiO₄] tetrahedra and [Si₂O₇] ditetrahedra that share common vertices, running parallel to the b-axis. The interspaces of the chains are filled by calcium, forming an infinite chain of [CaO₆] octahedra that also runs parallel to the b-axis. The three chains are stacked along the c-axis and result in acicular or fibrous triclinical wollastonite-1T. A powder X-ray diffraction (XRD) pattern suggests that the wollastonite used in this study is wollastonite-1T (Figure 1 a).^[24]

The morphology of the as-obtained wollastonite is illustrated by the scanning electron microscopy (SEM) images shown in Figure 1 b and c. Some of the fibrous wollastonites show a sheet-like morphology (Figure 1 b) that can only provide two surfaces for the growth of CNTs, while others show a stick-like morphology (Figure 1 c) that can provide more than two surfa-

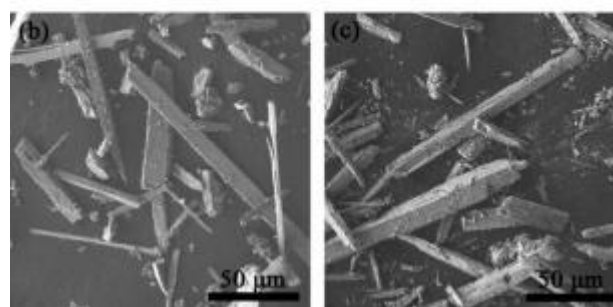
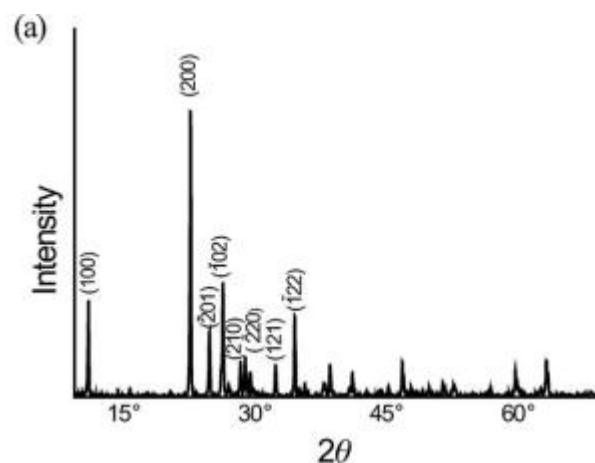


Figure 1. a) XRD pattern, and SEM images of b) the fibrous wollastonite sheets and c) wollastonite sticks used for aligned CNT growth.

ces for CNT growth. After impregnation, calcination, and reduction, Fe/Mo/wollastonite catalysts with different morphologies were obtained (see Experimental Section).

Aligned CNTs grown on wollastonite

When ethylene was introduced onto the Fe/Mo/wollastonite catalysts at the reaction temperature, CNTs were synchronously grown into array forms on their flat surfaces (Figure 2 a–f). Because only two flat surfaces were available for the sheet-like wollastonite, the structures obtained after the deposition of CNT arrays showed a leaf-like morphology, as shown in Figure 2 a and b. Figure 2 b and c shows that CNT arrays with a length of ca. 15 μm grew vertically on both sides of the wollastonite sheet, whose structure was well-preserved after the CNT synthesis. However, the CNT array was not so well aligned (Figure 2 d). With stick-like wollastonite, CNT arrays were deposited on each surface of the wollastonite and finally formed a brush-like structure (Figure 2 e and f), which is similar to structures obtained by the fabrication of CNT arrays on the surfaces of quartz,^[25] carbon,^[26] SiC,^[27] and aluminum silicate fibers.^[25]

The synthesis of aligned CNTs on other natural materials has been reported only seldom. The synchronous growth of CNTs into array structures reported here is mainly attributed to the strongly dispersed catalyst particles and proper growth window (including catalyst reduction, growth temperature, and carbon source).^[28] During the catalyst preparation process, the alkaline surface preferentially absorbed Fe³⁺ to form an

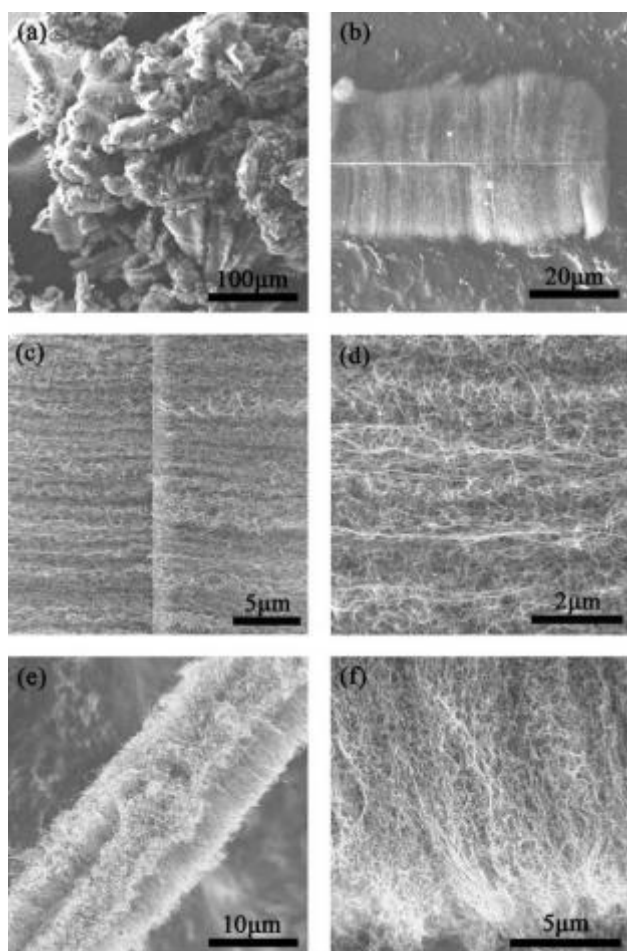


Figure 2. SEM images of a, b, c, d) leaf-like wollastonite/CNT hybrids obtained from fibrous wollastonite sheets, and e, f) brush-like wollastonite/CNT hybrids obtained from fibrous wollastonite sticks, after CVD at 700°C with ethylene.

Fe(OH)₃ layer. Fe³⁺ ions could then precipitate uniformly onto the wollastonite fibers. Moreover, the addition of molybdenum was intended to increase the stability of the iron nanoparticles. After calcination and reduction, as shown in Figure 3a, active catalyst particles were distributed uniformly on the surface of the fibrous wollastonite with a high density, estimated to be $8.5 \times 10^{13} \text{ m}^{-2}$. The catalyst particles showed small sizes, from several nanometers up to tens of nanometers, and they were effective for CNT growth in high density. The CNTs self-organized into an aligned morphology, as shown in Figure 2.

Structure of the as-grown aligned CNTs on wollastonite

The structure of the CNTs deposited on wollastonite is illustrated well by the transmission electron microscopy (TEM) image shown in Figure 4a. High-resolution TEM images (Figure 4b and c) show that the as-obtained CNTs exhibited clear graphite layers and few defects on the walls of the CNTs. There still were large amounts of few-walled CNTs (number of walls 2–6) in the as-grown CNT arrays (Figure 4a and c). The outer diameters of the CNTs showed a distribution ranging from 4 to

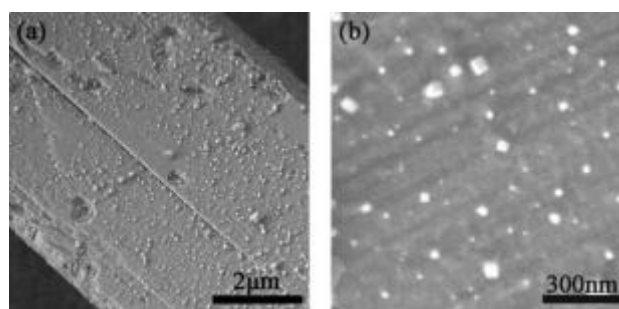


Figure 3. a, b) SEM images showing Fe/Mo catalyst particles on the surface of wollastonite after the reduction process.

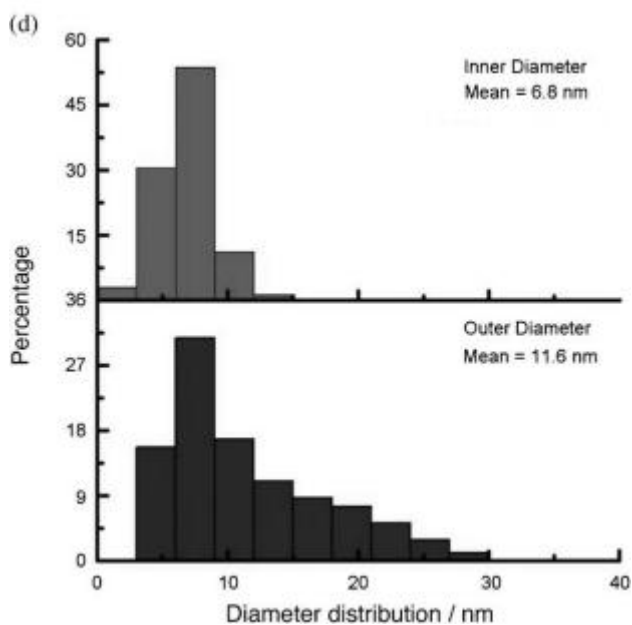
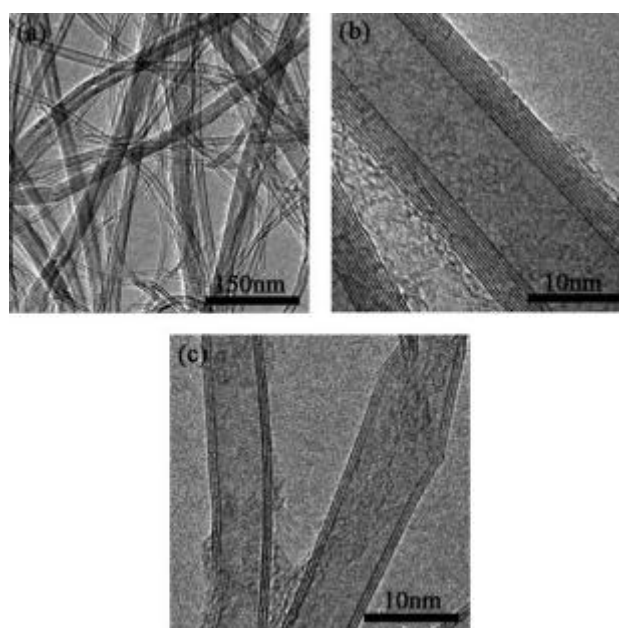


Figure 4. a) TEM image, and b, c) high-resolution TEM images. d) Distributions of the outer and inner diameters of the as-obtained CNTs.

30 nm, while the distribution of the inner diameters of the CNTs ranged from 4 to 12 nm, as shown in Figure 4d.

Thermogravimetric analysis (TGA) in air, shown in Figure 5a, indicated that about 30 wt% of the wollastonite/CNT hybrid corresponded to CNTs. The sharp and narrow derivative thermogravimetric (DTG) peak with a high ignition temperature (676.18°C) indicated that the obtained CNTs were of high quality. Raman spectroscopy was also used to macroscopically analyze the crystallization of the obtained CNTs. The ratio of the D band (1350 cm⁻¹, defect mode) to the G band (1585 cm⁻¹, graphite band) was low (0.54), revealing the high degree of crystallization of the CNTs (Figure 5b).

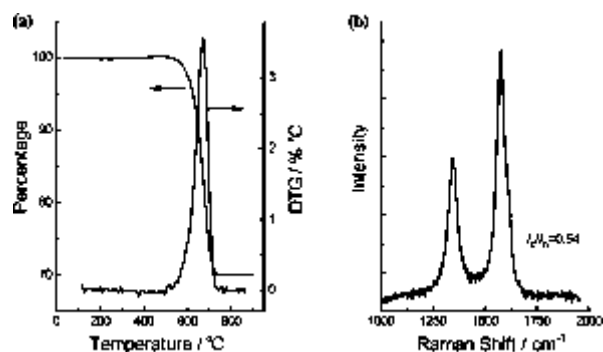


Figure 5. a) TGA curve, and b) Raman spectrum of the as-obtained wollastonite/CNT hybrids excited with a 514 nm laser, showing the D and G peaks ($I_D/I_G = 0.54$).

It is interesting to compare the properties of the CNTs obtained in the present research with those based on other natural materials. As shown in Table 2, compared with natural materials that were used as the catalyst directly, such as lava,^[6] garnet,^[11] and bentonite,^[12] CNTs on wollastonite were with smaller diameters and higher yields. For forsterite, diopside, magnesite, and brucite,^[14] only amorphous carbon or single-walled CNTs (SWCNTs) with low yields were obtained at the operated growth windows. When montmorillonite was used as catalyst support, multiwalled CNTs (MWCNTs) with relatively small diameters and high yields were obtained,^[16,29] but they were strongly entangled. With fly ash, entangled carbon nanofibers (CNFs) as well as MWCNTs with broad diameter distributions (10–200 nm) and high I_D/I_G values (0.83–1.28) were obtained, indicating that the CNTs were of low quality.^[17] Vermicu-

Table 2. CVD growth of nanocarbon materials on various natural minerals.							
Mineral	CVD temp. [°C]	Carbon source	Type	Diameter [nm]	I_D/I_G	Yield [$\text{g g}_{\text{cat}}^{-1} \text{h}^{-1}$]	Ref.
Lava	650–700	ethylene	CNF/MWCNT	30–200	0.66	0.18–0.26	[6]
Garnet	850	city gas	MWCNT	76	0.36–0.51	0.33–0.43	[11]
Bentonite	650	ethylene	MWCNT	5–40	/	0.40	[12]
Forsterite	800–900	methane	amorphous carbon	–	–	–	[14]
Diopside	800–900	methane	amorphous carbon	–	–	–	[14]
Magnesite	800–900	methane	SWCNT	1–1.8	0.14	–	[14]
Brucite	800–900	methane	SWCNT	1–1.8	0.14	–	[14]
Montmorillonite	700	acetylene	MWCNT	40–60	–	1.28	[29]
Montmorillonite	700	acetylene	MWCNT	25–35	–	–	[16]
Fly ash	700	ethylene	CNF/MWCNT	10–200	0.83–1.28	0.2–1.0 ^[a]	[17]
Vermiculite	900	methane	S/MWCNT	0.9–30	0.12–1.6	0.001–0.02 ^[a]	[30]
Vermiculite	650–750	ethylene	MWCNT array	4–14	1.06	5.25	[21], [31]
Wollastonite	700	ethylene	MWCNT array	4–30	0.54	0.86	This work

[a] Expressed in $\text{g g}_{\text{cat}}^{-1}$.

lite was also demonstrated to be a good catalyst support for the growth of CNTs. When the reaction was operated at 900°C using methane as the carbon source, entangled S/MWCNTs with small diameters and low yields were obtained.^[30] However, when the reaction was operated in the temperature range of 650–750°C and using ethylene as carbon source, MWCNT arrays with high yields were grown among the layers of vermiculite in an intercalated manner,^[31] but the value of I_D/I_G was 1.06; much higher than when grown on wollastonite, indicating the relatively high defect density of the obtained CNTs on vermiculite. In this work, with a good dispersion of iron particles formed on wollastonite by precipitation and reduction, aligned MWCNT arrays with small diameters (4–30 nm), low I_D/I_G values (0.54), and high yields (0.86 $\text{g g}_{\text{cat}}^{-1} \text{h}^{-1}$) were obtained. The CNTs were also much longer (15 μm).

Transformation into SiO₂/CNT hybrids

Wollastonite can be easily transformed into porous amorphous SiO₂ by reaction with hydrochloric acid at 50–60°C, and the as-obtained products with high surface areas can be used as raw materials for the production of silastics, catalyst support, and other materials. Accordingly, we used a HCl solution to transform the wollastonite/CNT hybrid into a SiO₂/CNT hybrid material. As demonstrated by energy-dispersive X-ray (EDX; Figure 6a), the product mainly consisted of C, O, and Si, with an O/Si molar ratio of 10.9:5.4 and minor amounts of Ca and Fe. This indicated that the well-crystallized wollastonite in the wollastonite/CNT hybrid was successfully transformed into SiO₂ after HCl treatment, as illustrated by the black arrow in Figure 6b. Because only a weak external force was applied that could not destroy the alignment, it was observed that after the reaction the CNTs were still in array form. TGA indicated that

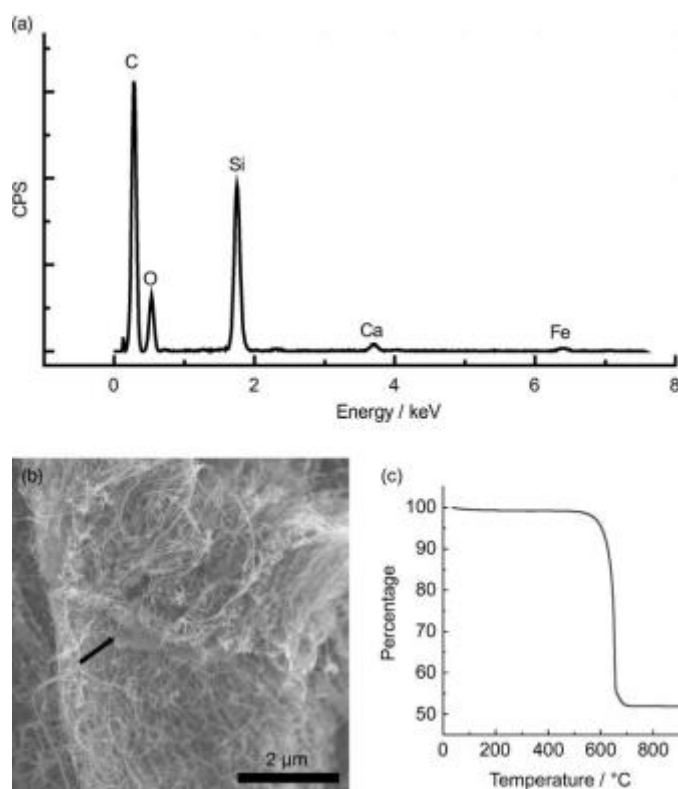


Figure 6. a) EDS spectrum, b) SEM image, and c) TGA curve of the SiO_2/CNT hybrid obtained after reaction with HCl.

the CNT content of the SiO_2/CNT hybrid had increased to 48.2% after the removal of CaO (Figure 6c).

To obtain the details of porous structure, both ex situ Hg penetration and N_2 adsorption measurements were carried out. As shown in Figure 7a, the pore sizes of the pristine wollastonite were concentrated around 10^3 – 10^4 nm, which can be attributed to interspaces among the packed fibrous wollastonites. When the CNTs arrays were synthesized on wollastonites, the volume of pores ranging from 2×10^3 to 3×10^5 nm as well as 30 to 2×10^3 nm showed a significant increase. The former can be assigned to enlarged spaces between the wollastonite/

CNT hybrids, while the latter probably corresponds to the spaces between the CNTs. For the SiO_2/CNT hybrids, the volume of pores with a large size decreased significantly, owing to a densification effect during the HCl treatment. However, the densification of the CNTs as well as pores formed by the removal of CaO from wollastonite obviously resulted in the increase of the volume of mesopores with a diameter of 5–50 nm. Figure 7b shows the pore size distribution below 10 nm, obtained by N_2 adsorption. The volume of pores ranging from 2 to 5 nm increased significantly after the deposition of CNTs, which can be assigned to the internal spaces among the CNTs. After treatment with HCl, the volume of pores (2–5 nm) of the SiO_2/CNT hybrids showed a further increase due to the removal of CaO, leading to the formation of large amounts of pores in wollastonite.

Furthermore, after deposition of CNTs the bulk density of the wollastonite sample decreased significantly, from 0.785 g cm^{-3} for the pristine material to 0.168 g cm^{-3} , while the total intrusion volume increased to $15.2 \text{ cm}^3 \text{ g}^{-1}$; about 17 times that of pristine wollastonite ($0.84 \text{ cm}^3 \text{ g}^{-1}$; Table 3). The porosity and Brunauer–Emmett–Teller (BET) specific surface area (SSA) of the wollastonite/CNT hybrids showed increases of 12.4% (from 65.9% to 74.1%) and 74.8% (from 32.1 to $56.1 \text{ m}^2 \text{ g}^{-1}$), respectively. The SSA of the CNTs in the hybrids was estimated to be $100.8 \text{ m}^2 \text{ g}^{-1}$. Furthermore, because of the densification effect during HCl treatment the bulk density of

Table 3. Comparison of the porous properties of wollastonite, wollastonite/CNT, and SiO_2/CNT .

Sample	Bulk density ^[a] [g cm^{-3}]	Porosity [%]	Total intrusion volume ^[b] [$\text{cm}^3 \text{ g}^{-1}$]	BET SSA ^[c] [$\text{m}^2 \text{ g}^{-1}$]
Wollastonite	0.785	65.9	0.84	32.1
Wollastonite/CNT hybrid	0.168	74.1	15.2	56.1
SiO_2/CNT hybrid	0.335	78.4	2.36	197.4

[a] Measured at 0.50 psia (1 psia = 6.894×10^3 Pa). [b] Measured by ex situ Hg penetration. [c] Measured by N_2 adsorption.

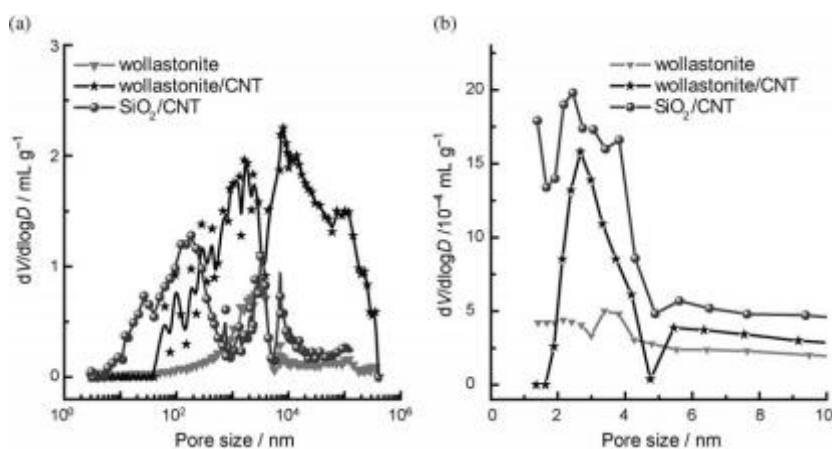


Figure 7. Pore size distributions obtained via a) ex situ Hg penetration and b) N_2 adsorption.

the obtained SiO_2/CNT hybrids increased to 0.335 g cm^{-3} while the total intrusion volume decreased to $2.36 \text{ cm}^3 \text{ g}^{-1}$. However, the porosity of the SiO_2/CNT hybrids showed a further increase to 78.4%, which can also be assigned to the formation of pores after the removal of CaO from wollastonite. For the same reason, the SSA of the SiO_2/CNT hybrids also showed a significant increase to $197.4 \text{ m}^2 \text{ g}^{-1}$, which is about six times that of the pristine wollastonite. The as-obtained porous SiO_2/CNT hybrids

with high SSA can be used as catalyst supports or for CO₂ absorption.^[32]

Purification of the aligned CNTs

The production of CNTs based on natural materials is very promising for providing low-cost, high-quality industrially available CNT products to develop large-scale applications. Thus, it is important to remove the natural materials after the CNT synthesis by a simple method. Here, to remove the SiO₂ from the SiO₂/CNT hybrids, a simple HF treatment was carried out to obtain purified CNT arrays. As shown in Figure 8a, the porous

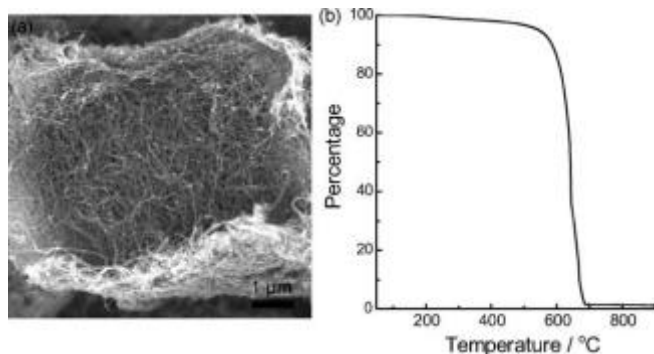


Figure 8. a) SEM image, and b) TGA curve of the purified aligned CNTs.

SiO₂ substrate was completely removed after reaction with HF, leaving a CNT array free of substrate. The purity of the as-purified CNT arrays was as high as 98.7%, as demonstrated by the TGA curve shown in Figure 8b. As a result, it is demonstrated that CNT arrays with high purity and small diameter can be easily produced at low costs by using natural wollastonite as catalyst support via CVD and a simple subsequent purification process.

Conclusions

Aligned CNTs of high quality and with small diameters were produced in a facile manner by using natural fibrous wollastonite as catalyst support, through the CVD process. The as-obtained wollastonite/CNT hybrids show leaf- or brush-like structures with a CNT content of 30.0%. They can be easily transformed into porous SiO₂/CNT hybrids by HCl treatment. The SiO₂/CNT hybrids obtained in this manner exhibit a structure with abundant pores and a high specific surface area of 197.4 m²g⁻¹. The CNT content of the SiO₂/CNT hybrids increased to 48.2% owing to the removal of CaO from the wollastonite. Furthermore, CNT arrays with a high purity of 98.7% were obtained following HF treatment, removing the SiO₂ from the SiO₂/CNT hybrids. This method provides new advanced materials based on natural materials with unique structure and properties that can be used as fillers, catalyst supports, or energy-absorbing materials.

Experimental Section

The wollastonite used here was mined in Jiangxi, PR China. Ball-milling was carried out to produce small fibrous wollastonite, which was then used as catalyst support. Fe(NO₃)₃·9H₂O (>99.0%, 5.0 g) and (NH₄)₆Mo₇O₂₄·4H₂O (>99.0%, 1.0 g) were dissolved in deionized water (100 mL). Wollastonite powder (20.0 g) was suspended in the solution to form a uniform suspension through strong stirring at 80°C for 6 h. After filtration, the filtrated cake was dried at 110°C for 12 h and was further calcined at 300°C for another 2 h yielding the fibrous Fe/Mo/wollastonite catalysts for CNT array production.

The preparation of the wollastonite/CNT hybrids was carried out by a catalytic CVD process. About 5.0 g of the Fe/Mo/wollastonite catalyst was sprayed uniformly at the center of a horizontal quartz tube inserted into a furnace at atmospheric pressure. The furnace was then heated under flows of Ar (600 mLmin⁻¹) and H₂ (50 mLmin⁻¹). When the temperature reached 700°C, C₂H₄ (100 mLmin⁻¹) was introduced into the reactor. The growth was maintained for 30 min at 700°C before the furnace was cooled to room temperature under protection of an Ar atmosphere. The products were then collected for further characterization.

The as-obtained wollastonite/CNT hybrids (1.0 g) were dispersed into deionized water (50 mL) under slight stirring. The suspension was heated to 55°C and hydrochloric acid (6.0 molL⁻¹) was dropped into the suspension to keep its pH below 0.15. The reaction was maintained for 40 min. After that, KOH solution (2.0 molL⁻¹) was used to adjust the pH of the solution to 4.0. The obtained suspension was filtrated and dried at 120°C for 1 h and then calcined at 700°C for 1 h. The as-obtained SiO₂/CNT hybrids were then collected and characterized.

Purification of the aligned CNTs was carried out by using HF to remove SiO₂ from the SiO₂/CNT hybrids. A sample of SiO₂/CNT hybrids (0.50 g) was put into a polyfluorotetraethylene pot containing 100 mL HF (3.0 molL⁻¹). The SiO₂/CNT hybrids were dispersed by slight stirring and the suspension was heated to 60°C and kept for 1 h. After that, the suspension was filtrated and dried at 120°C for another 1 h. Purified CNT arrays were obtained for further characterization.

The samples were characterized by using a JSM 7401F (JEOL Ltd., Tokyo, Japan) SEM instrument operating at 3.0 kV and a JEM 2010 (JEOL Ltd., Tokyo, Japan) TEM instrument operating at 120.0 kV. EDX analysis was performed by using a JSM-7401F apparatus with the analytical software INCA and an applied accelerating voltage of 15.0 kV. XRF analysis was carried out by using an XRF-1800 to obtain the composition of the pristine wollastonite. XRD patterns were recorded on a Rigaku D/max-RB diffractometer at 40.0 kV and 120 mA with Cu-Kα radiation. The carbon content was analyzed by TGA heated under air atmosphere with a temperature ramp rate of 10°Cmin⁻¹ using a Q500 device. Raman spectra were obtained with He-Ne laser excitation at 514 and 633 nm using a Renishaw RM2000. The pore size distribution of the samples was measured by an ex situ Hg penetration method. The BET specific surface area of all samples was measured by N₂ adsorption at liquid N₂ temperature by using a Micrometrics Flow Sorb II 2300.

Acknowledgements

The work was supported by the Natural Scientific Foundation of China (No. 20736004, No. 20736007, No. 2007AA03Z346), and the China National Program (No. 2006CB0N0702).

Keywords: carbon nanotubes · chemical vapor deposition · heterogeneous catalysis · nanostructures · natural materials

- [1] D. S. Su, *ChemSusChem* **2009**, *2*, 1009–1020.
- [2] a) M. M. Titirici, M. Antonietti, *Chem. Soc. Rev.* **2010**, *39*, 103–116; b) L. Lukyanova, R. Castangia, S. Franceschi-Messant, E. Perez, I. Rico-Lattes, *ChemSusChem* **2008**, *1*, 514–518.
- [3] a) M. Pumera, *Chem. Eur. J.* **2009**, *15*, 4970–4978; b) H. Zhang, G. P. Cao, Y. S. Yang, *Energy Environ. Sci.* **2009**, *2*, 932–943; c) G. Centi, S. Perathoner, *Eur. J. Inorg. Chem.* **2009**, 3851–3878.
- [4] a) K. P. Gong, F. Du, Z. H. Xia, M. Durstock, L. M. Dai, *Science* **2009**, *323*, 760–764; b) J. Liu, G. Z. Cao, Z. G. Yang, D. H. Wang, D. Dubois, X. D. Zhou, G. L. Graff, L. R. Pederson, J. G. Zhang, *ChemSusChem* **2008**, *1*, 676–697.
- [5] J. N. Coleman, U. Khan, W. J. Blau, Y. K. Gun'ko, *Carbon* **2006**, *44*, 1624–1652.
- [6] D. S. Su, X. W. Chen, X. Liu, J. J. Delgado, R. Schlogl, A. Gajovic, *Adv. Mater.* **2008**, *20*, 3597–3600.
- [7] a) J. Zhang, X. Liu, R. Blume, A. H. Zhang, R. Schlogl, D. S. Su, *Science* **2008**, *322*, 73–77; b) X. Liu, D. S. Su, R. Schlogl, *Carbon* **2008**, *46*, 547–549.
- [8] a) X. L. Pan, Z. L. Fan, W. Chen, Y. J. Ding, H. Y. Luo, X. H. Bao, *Nat. Mater.* **2007**, *6*, 507–511; b) X. L. Pan, X. H. Bao, *Chem. Commun.* **2008**, 6271–6281; c) P. Serp, E. Castillejos, *ChemCatChem* **2010**, *2*, 41–47.
- [9] S. S. Fan, M. G. Chapline, N. R. Franklin, T. W. Tombler, A. M. Cassell, H. J. Dai, *Science* **1999**, *283*, 512–514.
- [10] a) D. S. Su, X. W. Chen, *Angew. Chem.* **2007**, *119*, 1855–1856; *Angew. Chem. Int. Ed.* **2007**, *46*, 1823–1824; b) D. S. Su, A. Rinaldi, W. Frandsen, G. Weinberg, *Phys. Status Solidi B* **2007**, *244*, 3916–3919.
- [11] M. Endo, K. Takeuchi, Y. A. Kim, K. C. Park, T. Ichiki, T. Hayashi, T. Fukuyo, S. Linou, D. S. Su, M. Terrones, M. S. Dresselhaus, *ChemSusChem* **2008**, *1*, 820–822.
- [12] A. Rinaldi, J. Zhang, J. Mizera, F. Girgsdies, N. Wang, S. B. A. Hamid, R. Schlogl, D. S. Su, *Chem. Commun.* **2008**, 6528–6530.
- [13] A. Gomez-Avilés, M. Darder, P. Aranda, E. Ruiz-Hitzky, *Angew. Chem.* **2007**, *119*, 941–943; *Angew. Chem. Int. Ed.* **2007**, *46*, 923–925.
- [14] S. Kawasaki, M. Shinoda, T. Shimada, F. Okino, H. Touhara, *Carbon* **2006**, *44*, 2139–2141.
- [15] a) D. S. Su, X. W. Chen, G. Weinberg, A. Klein-Hofmann, O. Timpe, S. B. A. Hamid, R. Schlogl, *Angew. Chem.* **2005**, *117*, 5624–5628; *Angew. Chem. Int. Ed.* **2005**, *44*, 5488–5492; b) X. W. Chen, D. S. Su, S. B. A. Hamid, R. Schlogl, *Carbon* **2007**, *45*, 895–898; c) X. W. Chen, O. Timpe, S. B. A. Hamid, R. Schlogl, D. S. Su, *Carbon* **2009**, *47*, 340–343.
- [16] D. Gournis, M. A. Karakassides, T. Bakas, N. Boukos, D. Petridis, *Carbon* **2002**, *40*, 2641–2646.
- [17] O. M. Dunens, K. J. MacKenzie, A. T. Harris, *Environ. Sci. Technol.* **2009**, *43*, 7889–7894.
- [18] a) J. S. Qiu, Y. F. Li, Y. P. Wang, T. H. Wang, Z. B. Zhao, Y. Zhou, F. Li, H. M. Cheng, *Carbon* **2003**, *41*, 2170–2173; b) J. S. Qiu, Z. Y. Wang, Z. B. Zhao, T. H. Wang, *Fuel* **2007**, *86*, 282–286.
- [19] a) J. Q. Huang, Q. Zhang, F. Wei, W. Z. Qian, D. Z. Wang, L. Hu, *Carbon* **2008**, *46*, 291–296; b) Q. Zhang, J. Q. Huang, F. Wei, G. H. Xu, Y. Wang, W. Z. Qian, D. Z. Wang, *Chin. Sci. Bull.* **2007**, *52*, 2896–2902; c) J. M. Zhou, G. D. Lin, H. B. Zhang, *Catal. Commun.* **2009**, *10*, 1944–1947; d) P. Ndungu, Z. G. Godongwana, L. F. Petrik, A. Nechaev, S. Liao, V. Linkov, *Microporous Mesoporous Mater.* **2008**, *116*, 593–600.
- [20] a) M. Kumar, T. Okazaki, M. Hiramoto, Y. Ando, *Carbon* **2007**, *45*, 1899–1904; b) P. Ghosh, T. Soga, K. Ghosh, R. A. Afre, T. Jimbo, Y. And, *J. Non-Cryst. Solids* **2008**, *354*, 4101–4106.
- [21] Q. Zhang, M. Q. Zhao, Y. Liu, A. Y. Cao, W. Z. Qian, Y. F. Lu, F. Wei, *Adv. Mater.* **2009**, *21*, 2876–2880.
- [22] W. D. Zhang, I. Y. Phang, T. X. Liu, *Adv. Mater.* **2006**, *18*, 73–77.
- [23] N. I. Demidenko, L. I. Podzorova, V. S. Rozanova, V. A. Skorokhodov, V. Y. Shevchenko, *Glass Ceram.* **2001**, *58*, 308–311.
- [24] S. M. Salman, H. Darwish, E. A. Mahdy, *Mater. Chem. Phys.* **2008**, *112*, 945–953.
- [25] Q. Zhang, W. Z. Qian, R. Xiang, Z. Yang, G. H. Luo, Y. Wang, F. Wei, *Mater. Chem. Phys.* **2008**, *107*, 317–321.
- [26] N. Yamamoto, A. J. Hart, E. J. Garcia, S. S. Wicks, H. M. Duong, A. H. Slocum, B. L. Wardle, *Carbon* **2009**, *47*, 551–560.
- [27] A. Y. Cao, V. P. Veedu, X. S. Li, Z. L. Yao, M. N. Ghasemi-Nejhad, P. M. Ajayan, *Nat. Mater.* **2005**, *4*, 540–545.
- [28] Q. Zhang, W. P. Zhou, W. Z. Qian, R. Xiang, J. Q. Huang, D. Z. Wang, F. Wei, *J. Phys. Chem. C* **2007**, *111*, 14638–14643.
- [29] A. Bakandritsos, A. Simopoulos, D. Petridis, *Chem. Mater.* **2005**, *17*, 3468–3474.
- [30] F. C. C. Moura, R. M. Lago, *Appl. Catal. B: Environ.* **2009**, *90*, 436–440.
- [31] a) Q. Zhang, M. Q. Zhao, J. Q. Huang, Y. Liu, Y. Wang, W. Z. Qian, F. Wei, *Carbon* **2009**, *47*, 2600–2610; b) Q. Zhang, M. Q. Zhao, J. Q. Huang, J. Q. Nie, F. Wei, *Carbon* **2010**, *48*, 1196–1209; c) Q. Zhang, M. Q. Zhao, J. Q. Huang, F. Wei, *Powder Technol.* **2010**, *198*, 285–291.
- [32] S. Choi, J. H. Drese, C. W. Jones, *ChemSusChem* **2009**, *2*, 796–854.

Received: January 3, 2010

Published online on February 22, 2010